Response Letter

We are grateful for the reviewers' constructive and valuable comments and deeply appreciate their hard work and critical reading of our manuscript. We would also like to express our sincere gratitude for the deadline extension, which gave us the time needed to conduct a more thorough revision and additional reanalysis. Here we provide point-by-point responses to the 19 comments/suggestions raised by the two reviewers, denoted as [#1-1]–[#1-13] and [#2-1]–[#2-6], respectively. The original comments are italicized and shown in blue below. The line numbers in the comments refer to those in the original manuscript, while the line numbers denoted as "new line" refer to those in the revised manuscript. Revised sentences in the response below and the updated manuscript are indicated in red. In addition to responding to the reviewers, we have further refined the text and references, as summarized in the "Additional Amendments" section at the end of this letter.

Reply to Reviewer #1:

This manuscript provides valuable estimates of the river incision parameters n and K for soft sedimentary rocks, a lithology that is often underrepresented in global geomorphological datasets. The use of marine terrace ages as a proxy for long-term river incision rates (E) is an interesting alternative to the cosmogenic-radionuclide-based approaches used in previous studies to contruct ksn-erosion relationships. However, the manuscript requires major revisions to address a lack of methodological detail, unproven assumptions regarding knickpoint morphology, and insufficient clarity regarding the role of sea-level fluctuations.

Thank you very much for evaluating our manuscript. We have improved the original manuscript in accordance with your constructive, helpful comments and suggestions as follows.

Major comments:

#1-1 Transparency of the ksn–Erosion Derivation

The methodology for relating ksn to erosion rates (Sect. 4.2) is central to the parameter estimation, yet it lacks necessary detail.

- Location for sampling sites: In Figure 7, multiple data points of the same color represent different sections/reaches of a single river. The authors must explicitly describe and map the individual sites where these reach-scale incision rates were measured (e.g., following the format of Figure 1 in Leonard et al., 2023).

Leonard, J.S., Whipple, K.X., and Heimsath, A.M., 2023, Controls on topography and erosion of the north-central Andes: Geology, doi:10.1130/G51618.1.

We agree with the reviewer that accurately representing the location for sampling sites is crucial.

To address the reviewer's comment, we have explicitly identified and mapped the individual locations of each erosion rate data point presented in Fig. 7 for all six rivers in the Supplementary Material (Figs. S1–S6). These maps follow the format of Leonard et al. (2023)

as suggested. In this study, the erosion rate is calculated based on the summit level of the marine terrace, which was reconstructed by interpolating the highest elevations of multiple topographic profiles taken from preserved marine terrace surfaces. The profiles and their locations are also shown in Figs. S1–S6. As a representative example, Fig. S1 (the detailed map and profiles for the river No.1) is shown below.

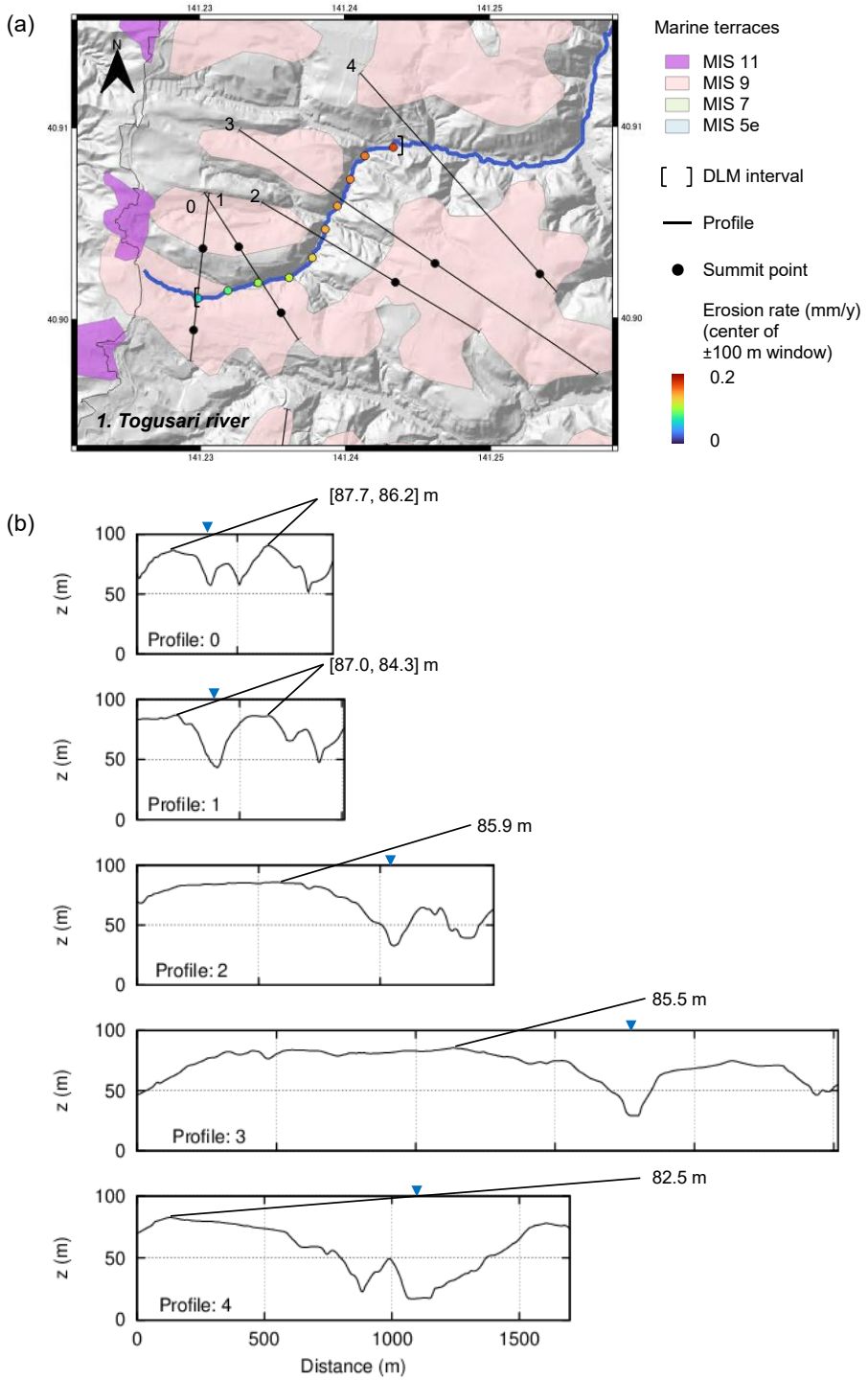

Figure S1: Data for River No.1. (a) Locations of summit levels (black points) extracted from profiles of the marine terrace surfaces (black lines) and representative points for estimated erosion rates (colored circles). (b) Profiles with riverbed locations (blue triangles).

We have also updated Fig. 2a to show the profile locations and their corresponding peak elevation points, adding the following sentence:

- New line 194–197

[Addition] The summit level of the marine terrace was reconstructed by interpolating the highest elevations from multiple topographic profiles extracted from preserved marine terrace surfaces (Fig. 2a; see Figs. S1–S6 for detailed maps and profiles). Where summit levels were comparable on both banks of the river, their average value was used.

[Revision]

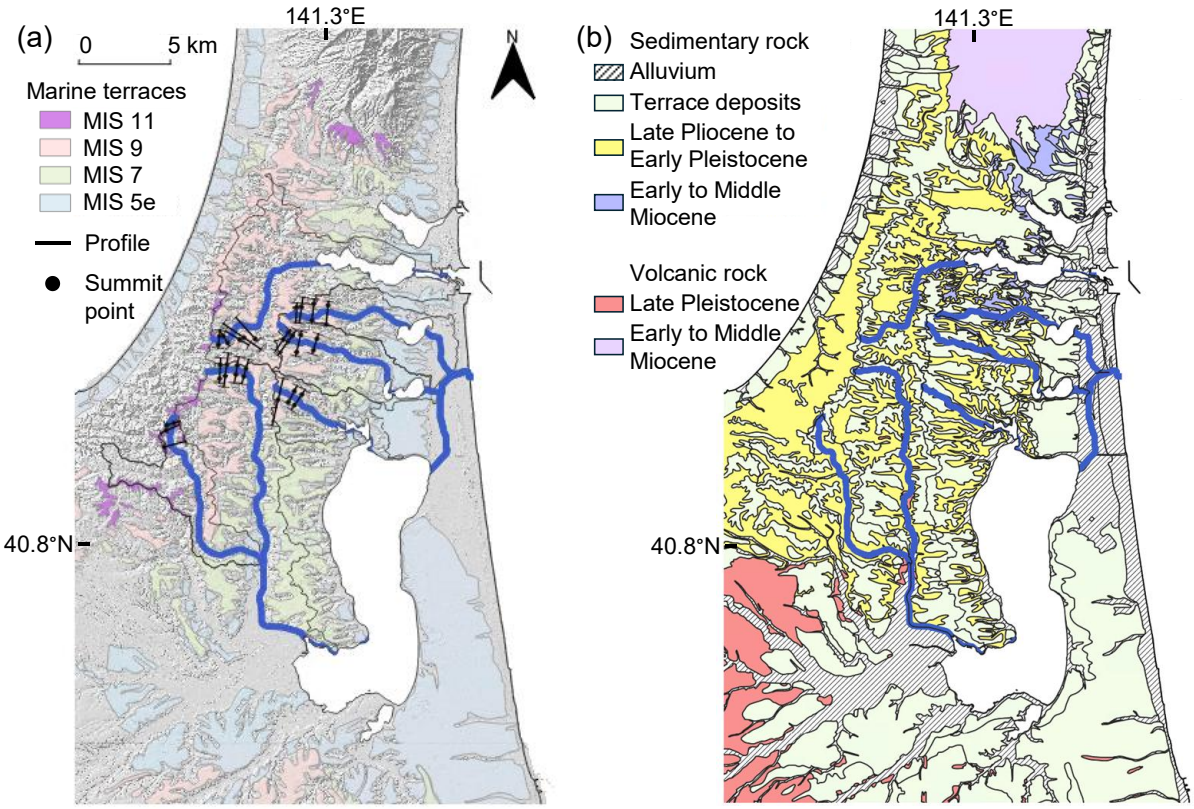

Figure 2: (a) Marine terraces and (b) geology of the study area. Marine terraces are based on Koike and Machida (2001). The summit levels extracted from profiles of the marine terrace surfaces were used for erosion rate estimates. Geological map is based on the 1:200,000 scale geologic map (AIST, 2025). Geological units are based on Kudo et al. (2020).

Regarding data processing, we have revised our methodology to ensure a more spatially uniform evaluation. Instead of using the log-bin averaged data (0.1 $\log_{10}$A intervals) as in the original manuscript, we now compare k_{sn} and erosion rates E at equal intervals of 200 m along the river channels. This follows the parameter estimation approach using fluvial terraces by Lague (2014), who reanalyzed the data of Lave and Avouac (2001) by comparing k_{sn} and E at constant spatial intervals (every 250 m). In accordance with this change, we have revised the corresponding sentences as follows:

- New line 198–199

[Addition] To ensure spatial consistency, E and k_{sn} were compared at equal intervals of 200 m along the river channels, following the approach for parameter estimation using strath terraces by Lague (2014).

- Line 226 (new line 279)

[Original] We then compared the long-term river incision rate E and the river steepness k_{sn} based on log-bin averaged data (Fig. 7).

[Revision] E and k_{sn} were compared at 200-m intervals along the river channels (Figs. 7a–c).

- Uncertainty consideration: Since incision rates (E) are derived from marine terrace heights (zt - zr - d) over time (Tt), any variation in tephra thickness (d) or terrace degradation introduces significant error. A formal uncertainty analysis for the regression in Figure 7 is required to assess the reliability of the resulting n and K values.

We appreciate this insightful suggestion. We have conducted a Monte Carlo simulation to quantify the uncertainty in the estimated erosion rates by propagating errors from each parameter (z_t, z_r, d, and T_t) through their assigned probability distributions. We have revised the relevant sentences and included the parameter settings as Table 2.

- Line 165–175 (new line 199–217)

[Original] Due to volcanoes in the nearby districts, tephra layers and loam … at one point. Based on previous research, d is assumed to be 12 m for MIS 11, 10 m for MIS 9, 5 m for MIS 7, and 2 m for MIS 5e terraces.

[Revision] To account for uncertainties in E (Eq. (9)), a Monte Carlo simulation with 10,000 iterations was performed based on the inherent probability distribution of all input parameters (Table 2). Elevation uncertainty was modeled as a Gaussian distribution based on DEM precision (0.3 m for DEM5A) in the detachment-limited reaches. The uncertainties in terrace age (T_t) and tephra thickness (d) were represented using uniform distributions derived from field observations.

T_t values were adapted from those reported by Matsu'ura et al. (2019) for the Kamikita Coastal Plain: 398 to 410 ka (MIS 11), 318 to 324 ka (MIS 9c), 230 to 235 ka (MIS 7e), 212 to 220 ka (MIS 7c), and 116 to 132 ka (MIS 5e). Furthermore, d values were derived from observed data of tephra layers and loam … Accordingly, a uniform thickness was assigned to each terrace stage (Table 2). This Monte Carlo approach enables the evaluation of the parameter reliability by accounting for uncertainties in summit level, riverbed elevation, tephra thickness, and marine terrace age.

Table 2: Probability distribution used for uncertainty analysis of erosion rate.

Parameter	Assigned distribution	Values

z_t	Summit level (m)	Gaussian	Mean: reconstructed summit level σ: standard deviation within 200 m interval
z_r	Riverbed (m)	Gaussian	Mean: elevation extracted from DEM σ: 0.3 m (standard error of DEM5A)
d	Tephra thickness (m)	Uniform	MIS 9: [7.0, 14.0], MIS 11: [10.5, 11.4]
T_t	Marine terrace age (ka)	Uniform	MIS 9c: [318, 324], MIS 11: [398, 410]

As a result, Fig. 7 and Table 5 (formerly Table 3) were revised as follows. In response to comment [#2-2], θ_{ref} was changed to 0.4, 0.5, and 0.6. Consistent with the original manuscript, the estimated value of n was nonlinear ($n > 1$) when all data points were used, whereas it was linear ($n \sim 1$) when averaged data for each detachment-limited reach were used.

[Revision]

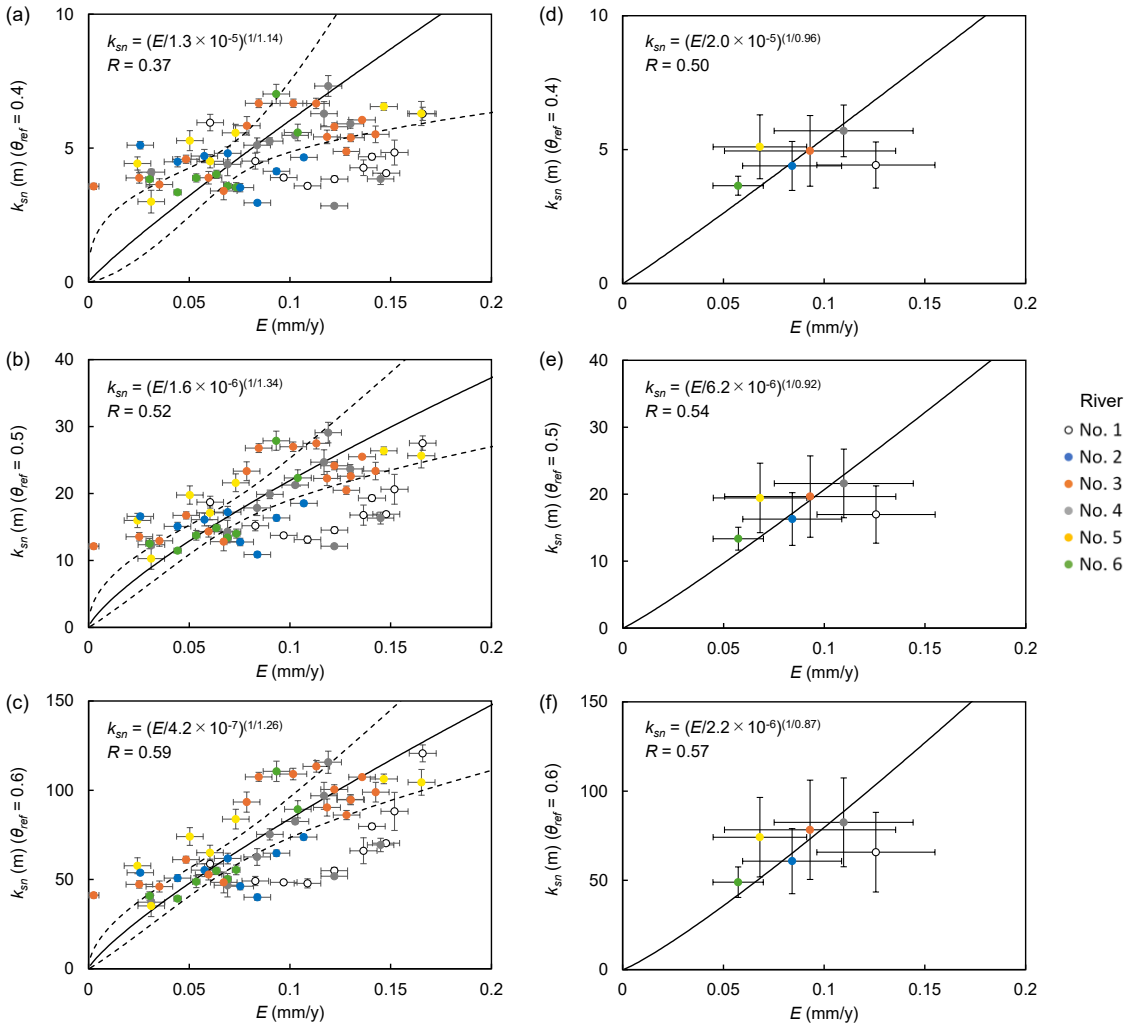

Figure 7: River incision rate versus channel steepness index k_{sn} within the detachment-limited reaches: (a-c) sampled at 200 m intervals and (d-f) averaged for each reach, both for θ_{ref} = 0.4, 0.5, and 0.6. Error bars denote $\pm 1\sigma$. The bold and dashed lines indicate the regression lines and their 90% confidence intervals.

Table 5: River incision parameters (n and K) and correlation coefficient estimated for each river (θ_{ref} = 0.5).

[Original]

No.	1	2	3	4	5	6
n (-)	0.82	1.14	2.10	1.59	1.48	2.07
K ($m^{0.1}\,y^{-1}$)	1.9×10^{-5}	3.7×10^{-6}	5.9×10^{-7}	2.5×10^{-6}	2.5×10^{-6}	1.0×10^{-6}
R	0.41	0.16	0.76	0.94	0.92	0.65

[Revision]

No.	1	2	3	4	5	6
n (-)	0.65	0.72	1.79	1.57	1.36	2.39
K	1.8×10^{-5}	9.9×10^{-6}	3.6×10^{-7}	8.2×10^{-7}	1.1×10^{-6}	1.1×10^{-7}
R	0.44	0.31	0.57	0.92	0.79	0.66

We have added the probability distributions of the estimated n and K as Fig. 8. To reflect these results, Sect. 4.2 has been revised as follows.

- Line 226–234 (new line 279–288)

[Original]

We then compared the long-term river incision rate E and the river steepness k_{sn} based on log-bin averaged data (Fig. 7). Using the data of all the rivers, we confirmed that there is a positive correlation between E and k_{sn} with a correlation coefficient of $R = 0.46$. The parameter values were obtained as n of 1.54 [0.86, 2.22] (90% confidence interval) and K of 2.4×10^{-6} [5.6×10^{-7}, 1.0×10^{-5}] ($m^{0.1}\,y^{-1}$).

Table 3 shows the parameter values obtained for each river. Although a relatively high correlation could be confirmed for rivers No. 3-6 ($R \geq 0.65$), values of K vary by almost nearly one order of magnitude. This variation may have been caused by the uncertainty of marine terrace surface z_t along the rivers; high-level marine terraces used for estimation of E (MIS 9 and MIS 11) are dissected by river and stream erosion (Fig. 2a). This can cause the large scatter in Fig. 7 for small incision rate, which correspond to upstream sections.

[Revision]

E and k_{sn} were compared at 200-m intervals along the river channels (Figs. 7a–c). A positive correlation between E and k_{sn} was observed across all θ_{ref} values. The correlation coefficient (R) increased with increasing θ_{ref}, ranging from 0.37 to 0.59. Across the range of $\theta_{ref} = 0.4$–0.6, the estimated n values consistently indicated a nonlinear relationship ($n > 1$) and fell within a narrow range from 1.14 to 1.34. In contrast, the estimated K varied over a considerably wider range from 4.2×10^{-7} to 1.3×10^{-5}. The 90% confidence intervals for these parameters were n = [0.94, 1.28], [1.15, 1.46], and [1.10, 1.36], and K = [1.0×10^{-6}, 2.9×10^{-6}], [1.1×10^{-6}, 2.9×10^{-6}] and [2.5×10^{-7}, 7.8×10^{-7}] for $\theta_{ref} = 0.4$, 0.5 and 0.6, respectively (Fig. 8 shows the results obtained at $\theta_{ref} = 0.5$).

Table 5 shows the parameter values obtained for each river. Although a relatively high correlation could be confirmed for rivers No. 3-6 ($R \geq 0.65$), values of K vary by nearly one order of magnitude. Similarly, the values of n exhibited inter-river variability; $n > 1$ for rivers Nos. 3–6, whereas $n < 1$ for rivers Nos. 1 and 2.

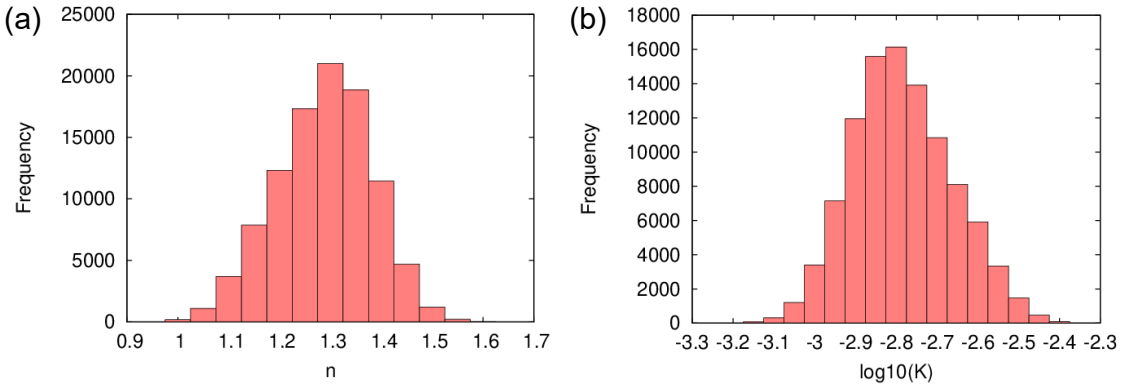

Figure 8: Probability distributions of n and K values estimated from 10,000 Monte Carlo simulations ($\theta_{ref} = 0.5$).

#1-2 Evidence for "Slope-Break" Knickpoints

The authors categorize the extracted knickpoints as "slope-break" type to argue for persistent incision driven by base-level fall.

- Missing analysis: Theoretically, slope-break knickpoints manifest as distinct changes in the slope of the slope-area curve (Figure 3b). However, no such shifts are clearly visible or quantitatively analyzed in the provided plots (Figure 4b).

- Extraction method: The current method of using local minimums of ksn with respect to chi can locate knickpoints but does not differentiate morphology-based knickpoint types, i.e. slope-break vs vertical step knickpoints. Without statistical or graphical proof of a slope change, these features could be vertical-step knickpoints highly relevant to simple lithological transitions.

Thank you for this insightful comment. We agree that the robust identification and classification of knickpoints are essential. As Reviewer #2 raised a similar concern regarding the knickpoint extraction, we have addressed this by implementing the statistical segment-fitting algorithm of Mudd et al. (2014). This new approach identifies the optimal concavity by fitting the χ-plot with multiple linear segments. Knickpoints are defined as the boundaries between adjacent segments and are classified as either vertical-step or slope-break knickpoints, based on the slope ratio of the regression lines (S_{ratio}) and the elevation difference (Z_{jump}) across the knickpoints.

Please refer to our detailed response to comment [#2-3] for the full methodological description (revised manuscript: new line 169–182) and the updated Table 4 (list of extracted knickpoints), which includes the S_{ratio} and Z_{jump} values for each knickpoint.

#1-3 Mechanism of Nonlinearity (n)

The authors suggest that sea-level fluctuations account for the nonlinear relationship (n = 1.54) between ksn and E.

Conceptual gap: The authors must explain the physical mechanism by which transient knickpoints from sea-level change result in a higher n value. Specifically, they should clarify if $n > 1$ is a result from the sea-level signal itself rather than an intrinsic physics of river incision process.

We agree with the reviewer that the relationship between sea-level fluctuations and n values needs to be explained more clearly from a physical perspective. In the revised manuscript, we propose that the observed $n > 1$ is likely an apparent nonlinearity resulting from transient landscape states, rather than being intrinsic to the physics of incision. This is based on the following two findings:

1. Regional knickpoints: The presence of slope-break knickpoints at similar elevations across multiple rivers indicates a common transient response to sea-level changes.
2. Scale dependency: While point-based analysis yielded $n > 1$, detachment-limited reach-averaged analysis (which smooths local transient signals) resulted in $n \sim 1$.

These results suggest that the observed nonlinearity is primarily an apparent effect caused by the presence of migrating knickpoints due to sea-level changes, leading to fluctuations in n. Although we consider sea-level-driven transience to be a major factor, we also acknowledge that the intrinsic physics of river incision, such as shear stress thresholds and abrasion, may simultaneously contribute to the observed nonlinearity. Their precise contributions remain to be evaluated in future work; however we have expanded our discussion to clarify the physical mechanisms that may cause the nonlinearity as follows:

- Line 242–252 (new line 301–328)

[Original]

In Sect. 4.2, the results of n (= 1.54) show a nonlinear relationship between incision rate E and river steepness k_{sn}. This is consistent with previous research conducted in various regions, where most estimates of n are between 1 and 2 (e.g., Ouimet et al., 2009; DiBiase et al., 2010; Lague, 2014; Harel et al., 2016; Campforts et al., 2020; Gallen and Fernandez-Blanco, 2021; Leonard et al., 2023). Additionally, we confirmed that the target rivers are impacted by eustatic sea-level change.

The migration of fluvial knickpoints migration due to sea-level change can cause the nonlinearity ($n > 1$) (Pavano, 2025). To reduce the effect of sea-level change (i.e., fluctuation caused by the knickpoints), we compared k_{sn} and E averaged for each river in common with Pavano et al. (2016). As a result, an almost linear value of $n = 1.01$ was obtained (Fig. 8). In particular, the trend of rivers in the same basin (No. 2-6) are quite similar, with a correlation factor of $R = 0.97$. Even excluding river No.1, the estimated parameter value is similar: $n = 1.02$ [0.86, 1.18]. This suggests that past sea-level fluctuations may account for the nonlinear relationship between k_{sn} and E. Note that the neglected effect of channel width is limited, since parameter estimation was performed in the limited upstream and midstream areas (Fig. 6).

[Revision]

In Sect. 4.2, the estimated values of n (1.14 to 1.34) indicate a nonlinear relationship ($n > 1$) between E and k_{sn} across θ_{ref} of 0.4–0.6. Specifically, for $\theta_{ref} = 0.5$ and 0.6 where $R \geqq 0.5$, the 90% confidence interval for n lie entirely above 1.1. This nonlinear relationship is consistent with previous research conducted in various regions, where most estimates of n are between 1 and 2 (e.g., Ouimet et al., 2009; DiBiase et al., 2010; Lague, 2014; Harel et al., 2016; Campforts

et al., 2020; Gallen and Fernandez-Blanco, 2021; Leonard et al., 2023). In addition, slope-break knickpoints occurred at similar elevations across multiple rivers, which do not correspond to boundaries of lithology or different DEM datasets.

Meanwhile, when we compared the averaged E and k_{sn} values within detachment-limited reaches, n was approximately 1 across all θ_{ref} values (n = 0.96, 0.92, and 0.87 for θ_{ref} = 0.4, 0.5, and 0.6; Figs. 7d-f). Furthermore, when river No.1 was excluded and only tributaries within the same drainage area (the Takase River) were compared, n was 1.05 with a higher R of 0.79.

These results suggest that the observed nonlinearity is likely an apparent effect caused by the presence of migrating knickpoints triggered by sea-level change (Pavano, 2025), rather than reflecting the intrinsic physics of river incision processes. Although most rivers yield $n > 1$, river Nos.1 or 2 exhibited $n < 1$. For river No.1, $n < 1$ possibly reflects the differences in watershed and downstream boundary conditions. Unlike other tributaries that flow into the large Lake Ogawara within the Takase River basin (867 km^2), river No.1 has a small drainage area (55.9 km^2) and flows into the small Takahoko pond. These contrasting base-level conditions can lead to different transient response at the catchment scale, causing fluctuations in n values. For river No.2, the presence of a lithological boundary, where the downstream lithology is more erodible than upstream lithology, may result in a lower n value.

Nevertheless, the intrinsic physics of river incision processes may also contribute to the observed nonlinearity. Such physical factors include shear stress thresholds, abrasion, plucking, and channel-width effects (Whipple et al., 2000), as well as tool and cover effects (Yamanashi and Naruse, 2025). The main target lithology comprises soft sedimentary rocks ($q_u \leqq 3$ MPa, as discussed in Sect. 5.2), where the tool and cover effects of riverbed gravel are likely minimal due to rapid disintegration into fine sediments; however, two possibilities remain: shear stress threshold and abrasion. In the small-scale catchments, the base flow discharge may be insufficient to exceed the critical shear stress required for bedrock incision. In addition, the abundance of sand derived from soft bedrock may cause suspended-load abrasion, which theoretically supports n values of ~5/3 (Whipple et al., 2000). Note that the neglected effect of channel width is limited, since parameter estimation was performed in the limited upstream and midstream areas (Fig. 6). While the relative contributions of these transient responses and physical processes require further comprehensive investigation, the estimated parameters represent robust time-averaged behavior integrated over multi glacial–interglacial cycles.

Minor comments:

#1-4 [Line 28-29]

Provide a citation for river incision as a primary driver of vertical erosion.

Thank you for your comment. We have added the citation as '*(e.g., Whipple, 2004)*'.

#1-5 [Line 43-45]

Provide a citation for the statement regarding parameter estimation from field data and the DL model.

Thank you for your comment. We have added the citation as '*(e.g., Kirby and Whipple, 2012; Lague, 2014)*'.

#1-6 [Line 63-65]

The connection between "safe waste transportation" and geological disposal is unclear. Clarify if the motivation is assessing the geological stability of the disposal site against future erosion, and specify the timeframe (e.g., "since the Late Quaternary").

As suggested by the reviewer, we have deleted the misleading term "safe waste transportation" (new line 68). Additionally, to clarify the motivation of the geological stability assessment, we have specified the timeframe and revised the relevant sentences in the Introduction as follows:

- Line 25-28 (new line 23–29)

[Original]

Prediction of long-term future landscape evolution is indispensable for social planning such as radioactive waste disposal and mine waste disposal. For example, the disposal facility for intermediate or high-level radioactive waste must be evaluated to ensure that it will remain isolated from the biosphere and humans for at least several thousand years (IAEA, 2011) to one million years (STUK, 2013).

[Revision]

Prediction of long-term landscape evolution is indispensable for social planning and infrastructure management, such as radioactive waste repositories, mine waste deposits, and landfills. In several fields, long-term assessments spanning 10^4–10^5 years are required to confirm geological stability; for instance, carbon dioxide capture and storage (~10,000 years: IPCC, 2005; Alcalde et al., 2018) and radioactive waste disposal (100,000 years for intermediate-level waste: e.g., SSM, 2008; NRA, 2021). To ensure reliable risk assessment for these facilities, including the evaluation of future erosion depths and their effects on groundwater flow systems, past landscape evolution since the Late Quaternary (i.e., the last glacial–interglacial cycle since 125 ka) must be elucidated.

The reference to IAEA (2011) and STUK (2013) have been replaced with the following references:

Alcalde, J., Flude, S., Wilkinson, M., Johnson, G., Edlmann, K., Bond, C. E., Scott, V., Gilfillan, S. M. V., Ogaya, X., and Haszeldine, R. S.: Estimating geological CO_2 storage security to deliver on climate mitigation, Nat. Commun., 9, 2201, https://doi.org/10.1038/s41467-018-04423-1, 2018.

IPCC: IPCC special report on carbon dioxide capture and storage, prepared by Working Group III of the Intergovernmental Panel on Climate Change, Metz, B., Davidson, O., de Coninck, H. C., Loos, M., and Meyer, L. (Eds.), Cambridge University Press, Cambridge, United Kingdom and New York, NY, USA, 431 pp., 2005.

NRA (Nuclear Regulation Authority): Interpretation of the location, structure and equipment for Category 2 waste disposal facilities (enacted on 27 November 2013, revised on 13

November 2019 and 29 September 2021), https://www.nra.go.jp/data/000069192.pdf (last access: 22 April 2026), 2021 (in Japanese).

SSM (Swedish Radiation Safety Authority): The Swedish Radiation Safety Authority's regulations concerning the protection of human health and the environment in connection with the final management of spent nuclear fuel and nuclear waste, SSMFS 2008:37, 2008.

#1-7 [Line 123-128]

In the context of Figure 3, the motivation for focusing exclusively on slope-break knickpoints should be described in a separate paragraph.

Thank you for this comment. We have added a separate paragraph and revised as follows:

[Original]

Slope-break knickpoints, on the other hand, develop spatially or temporally, which corresponds to regional-scale trends of lithologic heterogeneity and sea-level fall (e.g., Haviv et al., 2010; Kirby and Whipple, 2012; Boulton et al., 2020). In this study, we focused on the slope-break knickpoints, which cause an abrupt change in flow condition.

[Revision (new line 133–137)]

Herein, we focused on slope-break knickpoints because they represent channel response to regional-scale perturbations, such as lithologic heterogeneity and sea-level fall (e.g., Haviv et al., 2010; Kirby and Whipple, 2012; Boulton et al., 2020). Unlike vertical-step knickpoints, these features mark a fundamental shift in the channel gradient, leading to abrupt changes in flow conditions. By identifying these slope-break knickpoints, we can evaluate how regional-scale factors influence river incision parameters.

#1-8 [Line 144-147]

Clarify if the same analytical steps from previous research were followed. Additional details on how DEM-generated errors were avoided are necessary.

Thank you for this valuable comment on our methodology. We have revised the manuscript to clarify the consistency of our approach with previous research. We have also provided details on how we dealt with DEM-derived noise as follows:

[Original]

The measurement error (standard deviation) of the DEM is 0.3 m (DEM5A), 0.7 m (DEM5B), 1.4 m (DEM5C), and 5 m (10m DEM). In this study, we smoothed elevation data over a 500 m moving window and calculated averaged slopes on 5 m contours and log-bin averaged slopes.

[Revision (new line 156–162)]

In previous studies utilizing the USGS 10m DEM (root mean square error = 2.44 m; Gesch, 2007), Wobus et al. (2006) used moving-window sizes of 200 or 400 m, whereas Whipple et al.

(2007) suggested an optimal window size of 250 m. The DEM datasets used herein possess a maximum measurement error (standard deviation) of 5 m, with specific accuracies ranging from 0.3 m (DEM5A), 0.7 m (DEM5B), 1.4 m (DEM5C), to 5 m (10m DEM) (GIA, 2026). To ensure analytical consistency across the entire catchment and account for the largest measurement error, we smoothed elevation data using a 500-m moving window and calculated averaged slopes on 5 m contours and log-bin averaged slopes. We verified that no artificial knickpoints were generated at DEM tile boundaries.

We have also added the following reference:

Gesch, D.B.: The national elevation dataset, in: Digital Elevation Model Technologies and Applications: The DEM Users Manual, 2nd edn., edited by: Manue, D., American Society for Photogrammetry and Remote Sensing, Bethesda, Maryland, 99–118, 2007.

#1-9 [Line 147-148]

Clarify how the specific measurement errors for DEM5A/B/C were derived.

Thank you for this comment. The elevation accuracies (standard deviation) for DEM5A/B/C are provided by the Geospatial Information Authority of Japan (GIA). For example, the accuracy of DEM5A (0.3 m) was validated by the GIA by comparing airborne laser scanning data with ground control points. We have added the following citation in new line 160:

GIA (Geospatial Information Authority of Japan): Methods for creating elevation tiles and elevation values displayed on GSI Maps, https://maps.gsi.go.jp/development/hyokochi.html (last access: 15 April 2026), 2026 (in Japanese).

#1-10 [Line 158-159]

The regression ln(E) = a ln(ksn) + b is a standard derivation of the stream power law but requires a citation (e.g., Leonard et al., 2023). Detailed equations should be introduced in the Methods section.

Thank you for this comment. We have added detailed equations and the citations as follows:

[Revised (new line 183–189)]

In the third step, the values of n and K were estimated. Within the detachment-limited reaches, the relationship between E and k_{sn} is expressed as:

$$E = K k_{sn}^{n} \, . \tag{6}$$

Taking the natural logarithm of Eq. (7) allows n and K to be estimated via the regression analysis of E and k_{sn} (e.g., Leonard et al., 2023):

$$\ln(E) = n \ln(k_{sn}) + \ln(K) \, , \tag{7}$$

where n and $\ln(K)$ represent the slope of the regression line and the intercept, respectively.

#1-11 [Line 196]

The statement that "θ is approximately 0.4" is contradicted by River No. 2, which has a reported concavity of θ = 0.59.

Thank you for this insightful comment. As Reviewer #2 raised a concern regarding the θ estimation, we have reanalyzed the concavity using the statistical segment-fitting algorithm (Mudd et al., 2014).

Our updated analysis yielded a regional reference concavity (θ_{ref}) of 0.44 ± 0.10 (standard deviation). Although the optimal θ for individual rivers varies (ranging from 0.18 to 0.59), the regional mean is consistent with typical values for steady-state channels (0.35 to 0.6).

Please refer to our detailed response to comment [#2-3] and revised manuscript (new line 239–242).

#1-12 [Line 211-213]

The authors attribute knickpoints to base-level fall. They should specify if this is related to eustatic sea-level changes or accelerated incision. Eustatic changes do not necessarily lead to upstream-propagating transient knickpoints; the authors should add explicit evidence of slope-break changes.

Thank you for your comment. In the response to comment [#2-2] from Reviewer #2, we have added a new table (Table 3) summarizing the knickpoint types, along with and the elevation and slope change values across each knickpoint.

As shown in the table, all identified knickpoints are categorized as slope-break knickpoints. With the exception of one knickpoint in river No.2, these knickpoints do not coincide with the boundaries of lithology or different DEMs. As the sign of the slope change (S_{ratio}) across the knickpoints is not uniform, they may not all represent simple upstream-propagating transient signals as suggested by the reviewer. Meanwhile, the knickpoints are located at similar elevations in multiple rivers, indicating a significant regional response to sea-level changes.

In our revised discussion (Sect. 5.1), we emphasized that these features represent a transient response to sea-level change, which contributes to the observed n values, as detailed in our response to your earlier comment [#1-3].

#1-13 [Line 306-308]

Elaborate on the "benefits" for radioactive waste disposal. For instance, explain how confining K and n allows for the prediction of maximum erosion depth over a 100,000-year safety assessment period.

Thank you for your comment. As suggested by the reviewer, we have elaborated on the benefits for radioactive waste disposal as follows:

[Revision (new line 383–391)]

These results represent long-term average erosion trends integrated over multiple glacial–interglacial cycles (since MIS 9 or 11). Consequently, the estimated n and K values are considered to reflect integrated values that account for past temporal variations in external forcing, such as climate and sea-level changes. For long-term safety assessments, such as those required for radioactive waste disposal, these parameters serve as a basis for time-dependent simulations of future landscape evolution over a glacial–interglacial cycle (~10^4 to 10^5 years). Such simulations can be implemented using mixed DL and TL models, incorporating these time-varying external forcing and additional geomorphic processes, such as hillslope and coastal sediment transport (e.g., Salles et al., 2018). Using the estimated n and K values as the baseline, this approach could enable the reliable prediction of not only the maximum erosion depth, but also the spatial distribution of erosion across the site and its subsequent effects on groundwater flow systems.

Reply to Reviewer #2, Professor Carole Petit

The authors combine morphometric analyses with independent estimates of river incision rates (from marine terrace dating) to infer long-term erosion rates in the Kamikita peninsula in Japan.

From these analyses, they infer Stream Power Law (SPL) parameters such as the concavity index and the slope exponent n, which appears to be different from 1, implying a non-linear dependency of erosion rate on channel slope. Moreover, this study allows them to quantify bedrock erodibility, and hence to constrain all parameters that can be used to model long-term landscape erosion with the SPL.

The approach combining independent morphometric analyses and river incision rate estimates from ^{10}Be dating of marine terraces is interesting. The paper is well written and well illustrated; however, it lacks some discussion on the impact of the chosen methodology on the results. I think it can be accepted after a round of moderate to major revisions.

Thank you very much for evaluating our manuscript. We have improved the original manuscript in accordance with your constructive, helpful comments and suggestions as follows.

Major comments:

#2-1

I don't understand why the paper opens with a statement on the importance of erosion estimates for nuclear waste disposal. I am well aware that erosion can be a threat to the safety of waste disposal sites, but over time periods of 100 ka to 1 Ma, there can be many other parameters that will modulate erosion rates, such as climate and sea-level changes. I think that such erodibility estimates are valid only for a short period of time, corresponding to the present-day situation. It should not be forgotten that the K parameter in the SPL includes both bedrock erodibility and external factors such as precipitation rates.

We sincerely appreciate and agree with the reviewer's insightful comments regarding the influence of external factors on the K parameter, in addition to bedrock erodibility. First, we would like to clarify that our estimation is not based on cosmogenic nuclides (e.g., ^{10}Be), which typically reflect relatively short-term erosion rates (approximately 10^3 years in tectonically active regions such as Japan). Instead, we utilized marine terrace ages to derive long-term average incision rates over the Late Quaternary (10^5 years). As the reviewer correctly noted, the K parameter is modulated by external factors such as climate and sea-level changes. However, by utilizing marine terrace data spanning multiple glacial-interglacial cycles, our estimated parameters provide time-averaged values that incorporate the past temporal variations, capturing the long-term representative behavior of the system.

In accordance with the reviewer's suggestions, we have broadened the scope of the Introduction section to include various types of social planning and infrastructure management. We have also refined the target timescale, focusing on the Late Quaternary, and emphasized the geomorphological significance of this study: complementing global geomorphological datasets for soft sedimentary rocks and proposing an alternative approach to estimating long-term incision parameters using marine terraces. Furthermore, we have revised the Conclusion section to clarify how these parameters can be used to predict long-term landscape evolution.

・ Line 25−28 (new line 23−29)

[Original]

Prediction of long-term future landscape evolution is indispensable for social planning such as radioactive waste disposal and mine waste disposal. For example, the disposal facility for intermediate or high-level radioactive waste must be evaluated to ensure that it will remain isolated from the biosphere and humans for at least several thousand years (IAEA, 2011) to one million years (STUK, 2013). Among various landscape processes, river incision is one of the main drivers of landscape evolution and can cause large vertical erosion.

[Revision]

Prediction of long-term landscape evolution is indispensable for social planning and infrastructure management, such as radioactive waste repositories, mine waste deposits, and landfills. In several fields, long-term assessments spanning 10^4–10^5 years are required to confirm geological stability; for instance, carbon dioxide capture and storage (~10,000 years: IPCC, 2005; Alcalde et al., 2018) and radioactive waste disposal (100,000 years for intermediate-level waste: e.g., SSM, 2008; NRA, 2021). To ensure reliable risk assessment for these facilities, including the evaluation of future erosion depths and their effects on groundwater flow systems, past landscape evolution since the Late Quaternary (i.e., the last glacial–interglacial cycle since 125 ka) must be elucidated.

・ Line 53−66 (new line 54–71)

[Original]

However, there are two problems with the above studies. First, previous research ($q_u \geq 15$ MPa: Haag and Schoenbohm, 2025) lacks data of soft sedimentary rocks. This is especially important for Japan where over 50% of the surface geology consists of Paleogene and Neogene sedimentary rocks (NUMO, 2021). Nevertheless, river incision parameters and its relationship with q_u have not been discussed for soft sedimentary rocks with q_u = 1–10 MPa. Second, previous parameter estimations have primarily relied on basin average denudation rates derived from cosmogenic beryllium-10 (^{10}Be) in quartz grains from river sediments. However, it is difficult to measure the ^{10}Be concentration for sedimentary rocks in humid and tectonically active regions like Japan due to the lack of quartz and the diversity of topographic deformation and sedimentation-erosion processes (AIST, 2016). In such regions, the ^{10}Be measurement is appropriate for quartz-rich rocks, such as granite (e.g., Takahashi et al., 2023). Parameter estimations have been also conducted assuming a topographic steady state (e.g., Snyder et al., 2000; Kirby and Whipple, 2001; Duvall et al., 2004). However, many environments have not yet attained a steady state (Bishop et al., 2005; Campforts and Govers, 2015; Vanacker et al., 2015; Armitage et al., 2018). Especially in coastal areas, which are preferable for geological disposal in terms of safe waste transportation (METIJ, 2017), the landscape has been drastically changed due to periodic sea-level change. Very a few studies (e.g., Lague, 2014) address this issue by using reach incision rates based on fluvial terraces.

[Revision]

However, there are two problems with the above studies. First, previous research ($q_u \geq 15$ MPa: Haag and Schoenbohm, 2025) lacks data of soft sedimentary rocks. This is especially important for tectonically active regions like Japan where over 50% of the surface geology consists of

Paleogene and Neogene sedimentary rocks (NUMO, 2021). Nevertheless, river incision parameters and its relationship with q_u have not been discussed for soft sedimentary rocks with q_u = 1–10 MPa. Second, previous parameter estimations have primarily relied on basin average denudation rates derived from cosmogenic radionuclides (CRN), such as beryllium-10 (^{10}Be) in quartz grains from river sediments. However, it is difficult to measure the ^{10}Be concentration for sedimentary rocks in humid and tectonically active regions like Japan due to the lack of quartz and the diversity of topographic deformation and sedimentation-erosion processes (AIST, 2016). In such regions, the ^{10}Be measurement is appropriate for quartz-rich rocks, such as granite (e.g., Takahashi et al., 2023). Furthermore, CRN-derived denudation rates typically reflect relatively short-term durations, which are roughly inversely proportional to the incision rate (Lague, 2014). Therefore, CRN-derived denudation rates reflect average timescales of 10^5 years in active regions with erosion rates of several mm ky^{-1}, but only 10^2–10^3 years in tectonically active regions with several m ky^{-1} erosion (von Blanckenburg, 2006). Another conventional approach is to assume a topographic steady state (e.g., Snyder et al., 2000; Kirby and Whipple, 2001; Duvall et al., 2004). However, many environments have not yet attained a steady state (Bishop et al., 2005; Campforts and Govers, 2015; Vanacker et al., 2015; Armitage et al., 2018). Especially in coastal areas, the landscape has been drastically changed due to periodic sea-level change. Thus, as Lague (2014) noted, deriving locally measured incision rates from dated terraces remains one of the least potentially biased methods for quantifying long-term incision. However, only a few studies (e.g., Lague, 2014) address this issue by using reach incision rates based on strath terraces.

- Line 303−308 (new line 383–391)

[Original]

Although the estimation of long-term k_{sn} and E includes uncertainty (i.e., the formation age of river and the marine terrace surface), this study shows a similar trend of incision parameters for soft sedimentary rocks to more consolidated rocks in the previous global compilations. These results show the average trend of long-term erosion after MIS 9 or MIS 11. The obtained parameters are beneficial to perform predictions of long-term landscape evolution in the safety assessment of such as radioactive waste disposal. However, as we mentioned earlier, there is uncertainty due to the past sea-level change and the estimation error of marine terrace elevations.

[Revision]

These results represent long-term average erosion trends integrated over multiple glacial–interglacial cycles (since MIS 9 or 11). Consequently, the estimated n and K values are considered to reflect integrated values that account for past temporal variations in external forcing, such as climate and sea-level changes. For long-term safety assessments, such as those required for radioactive waste disposal, these parameters serve as a basis for time-dependent simulations of future landscape evolution over a glacial–interglacial cycle (~10^4 to 10^5 years). Such simulations can be implemented using mixed DL and TL models, incorporating these time-varying external forcing and additional geomorphic processes, such as hillslope and coastal sediment transport (e.g., Salles et al., 2018). Using the estimated n and K values as the baseline, this approach could enable the reliable prediction of not only the maximum erosion depth, but also the spatial distribution of erosion across the site and its subsequent effects on groundwater flow systems.

In addition to the references mentioned in our response to comment [#1-6], we have added the following reference:

von Blanckenburg, F.: The control mechanisms of erosion and weathering at basin scale from cosmogenic nuclides in river sediment, Earth Planet. Sc. Lett., 242, 224–239, https://doi.org/10.1016/j.epsl.2005.11.017, 2006.

#2-2

Why did you choose to examine only the east-draining rivers, which seem to have a short detachment-limited portion, and not the west-draining ones, which are shorter and presumably steeper? The lithology appears to be similar and marine terraces are also present on the western side.

We appreciate the reviewer's insightful comment regarding the west-draining rivers. While the western side has a similar lithology and steep topography, these rivers were excluded from our analysis due to the lack of preserved marine terraces in their upstream areas, as shown in the figure below (red line: Arito and Chigusabashi rivers). Consequently, we focused our study on the east-draining rivers to ensure the robustness of our *n* and *K* estimates.

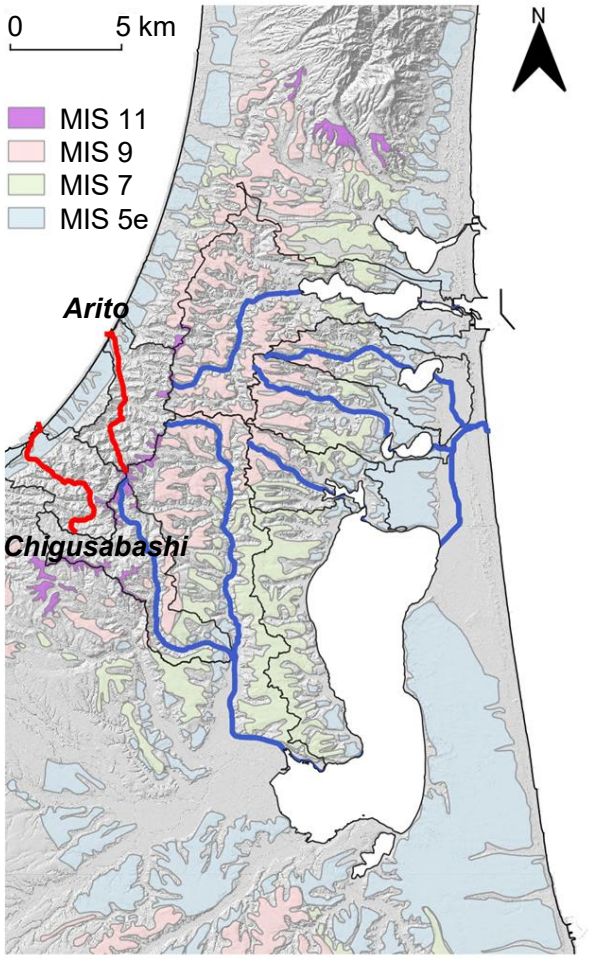

#2-3

The R coefficient of the chi-plot seems almost insensitive to variations in the concavity index theta (Figure 5), varying only between 0.95 and 1 for theta between 0 and 1. In my opinion, this reveals that the theta value is poorly constrained. Furthermore, if slope-break knickpoints are present in the channel profiles, a more sophisticated method should be used, with several line segments in the chi plot to infer the theta value while accounting for the different segments (https://lsdtopotools.github.io/LSDTT_documentation/LSDTT_chi_analysis.html). Ideally, the regional theta value should not be the average of individual estimates, but should instead be inferred by inversion from all channels together.

In accordance with this comment, we have reanalyzed the concavities and knickpoints using the statistical segment-fitting algorithm of Mudd et al. (2014), which is used in LSDTopoTools. We have revised the sentences in the Method section as follows.

- Line 155–157 (new line 169–182)

[Original]

Using a reference basin area of A_0 = 1 m^2, we estimated θ as the value providing the best linear fit between χ and z. $k_{sn} = SA^{\theta_{ref}}$ was calculated using θ_{ref}, the regional mean of θ. Knickpoints were extracted as the local minimum points of k_{sn} with respect to χ (Gailleton et al., 2019).

[Revision]

Using a reference basin area of A_0 = 1 m^2, the concavity index (θ) and knickpoint locations were estimated using a statistical segment-fitting algorithm (Mudd et al., 2014). In this algorithm, the optimal θ is evaluated in χ space by minimizing the corrected Akaike Information Criterion (AICc) across all possible contiguous channel segments.

$$\mathrm{AICc} = \mathrm{AIC} + \frac{2k(k+1)}{N-k-1}, \quad \mathrm{AIC} = 2k + \frac{RSS}{\sigma_z^2} \tag{6}$$

where N is the number of channel nodes, s is the number of segments ($k = 2s$), RSS is the residual sum of squares between data points and regression lines, and σ_z is the standard deviation of elevation measurements, including geomorphic noise. In this study, we used DEM5A (standard deviation: 0.3 m) in detachment-limited reaches, and σ_z was conservatively set to 0.6 m. A bootstrapping method was employed with 1,000 independent trials to evaluate the robustness of the results In this method, channel nodes were randomly skipped using a uniform distribution ranging from 0 to 2 × n_{sk}. Following Gailleton et al. (2019), n_{sk} was set to 1. θ_{ref} was determined using a collinearity test that minimized the sum of AICc values across all analyzed rivers. Knickpoints were defined as boundaries between adjacent segments. Knickpoint type was classified using the slope ratio of regression lines (S_{ratio}) and elevation difference (Z_{jump}) across these boundaries: large Z_{jump} with a minimal change in S_{ratio} indicates a vertical-step knickpoint, whereas a significant change in S_{ratio} with negligible Z_{jump} indicates a slope-break knickpoint. In accordance with Gailleton et al. (2019), knickpoints were extracted using the optimal θ specific to each river.

Accordingly, we have refined the bedrock section exhibiting detachment-limited like behaviors and updated the Results section, Figs. 4 and 5, and Table 2 as follows.

- Line 194–202 (new line 239–246)

[Original]

Estimated values of concavity index (θ) are summarised in Table 2. For all rivers, optimal θ achieved the linear regression of χ plots with high correlation coefficients of $R \sim 1$ (Fig. 5), which manifests DL-like behaviour in the upstream and midstream sections. Although θ ranges from 0.11 to 0.59, θ is approximately 0.4 except for small rivers of $A < 25$ km^2 (No. 2, 3, 4), which is the general range of steady-state channels (θ = 0.35–0.6: Kirby and Whipple, 2012). Notably, θ of river No. 6, whose formation age (MIS 11) is the oldest, is close to 0.45, a typical value for reference concavity index (e.g., Wobus et al., 2006). Snyder et al. (2003) indicates that even considering sea-level changes, a quasi-steady-state condition has been achieved in the upper parts of the channel. Therefore, although small channels tend to fluctuate from their mouths to their divides reflecting sea-level change, it can be assumed that the other rivers have approached to the quasi-steady state in the upstream section. In subsequent calculations, we analyzed k_{sn} based on θ_{ref} = 0.45.

[Revision]

The θ values estimated for detachment-limited reaches are summarised in Table 3 and Fig. 5. The optimal θ values for each river range from 0.18 to 0.59 (Fig. S8 shows the AICc values). Meanwhile, θ_{ref} was estimated to be 0.44 ± 0.10 (standard deviation) using the collinearity test (Fig. 5b), which lies within the general range of steady-state channels (θ = 0.35–0.6: Kirby and Whipple, 2012) and closely aligns with the typical reference concavity of 0.45 (e.g., Wobus et al., 2006). Snyder et al. (2003) indicates that even considering sea-level changes, a quasi-steady-state condition has been achieved in the upper parts of the channel. Therefore, although the target rivers tend to fluctuate from their mouths to their divides reflecting sea-level change, it can be assumed that they have approached the quasi-steady state in the upstream section. However, as θ_{ref} can impact the estimation of river incision parameters, we evaluated k_{sn} using θ_{ref} values of 0.4, 0.5, and 0.6 to ensure robustness.

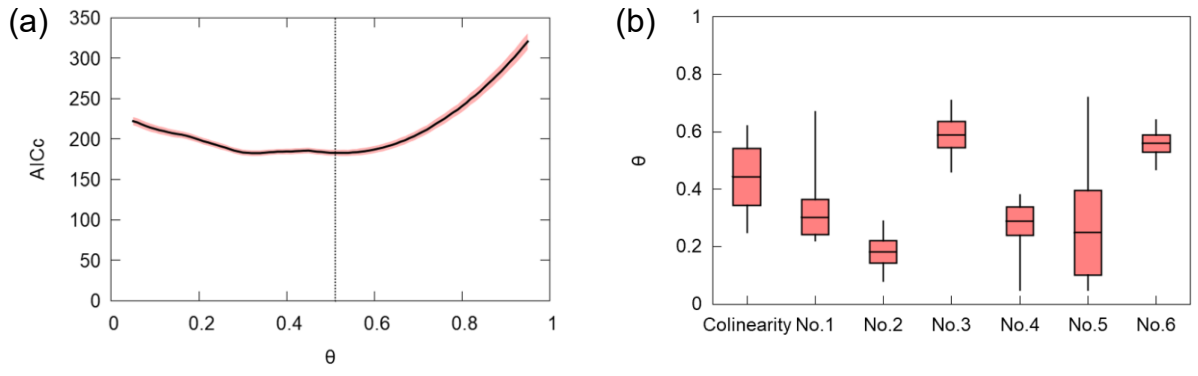

Figure 5: (a) AICc values for the regional collinearity test and (b) the distribution of optimal θ for regional and individual river basins. In (a), the solid line and shaded red area indicate the mean and ±1σ (standard deviation) interval for 1,000 bootstrap trials. In (b), the whiskers indicate the range between minimum and maximum values, while the boxes represent the mean and ±1σ interval.

[Original]

Table 2: Formation ages and concavity indices.

No.	1	2	3	4	5	6
Formation Age	MIS 9	MIS 9	MIS 9	MIS 9	MIS 9	MIS 11
θ	0.35	0.59	0.18	0.16	0.35	0.44

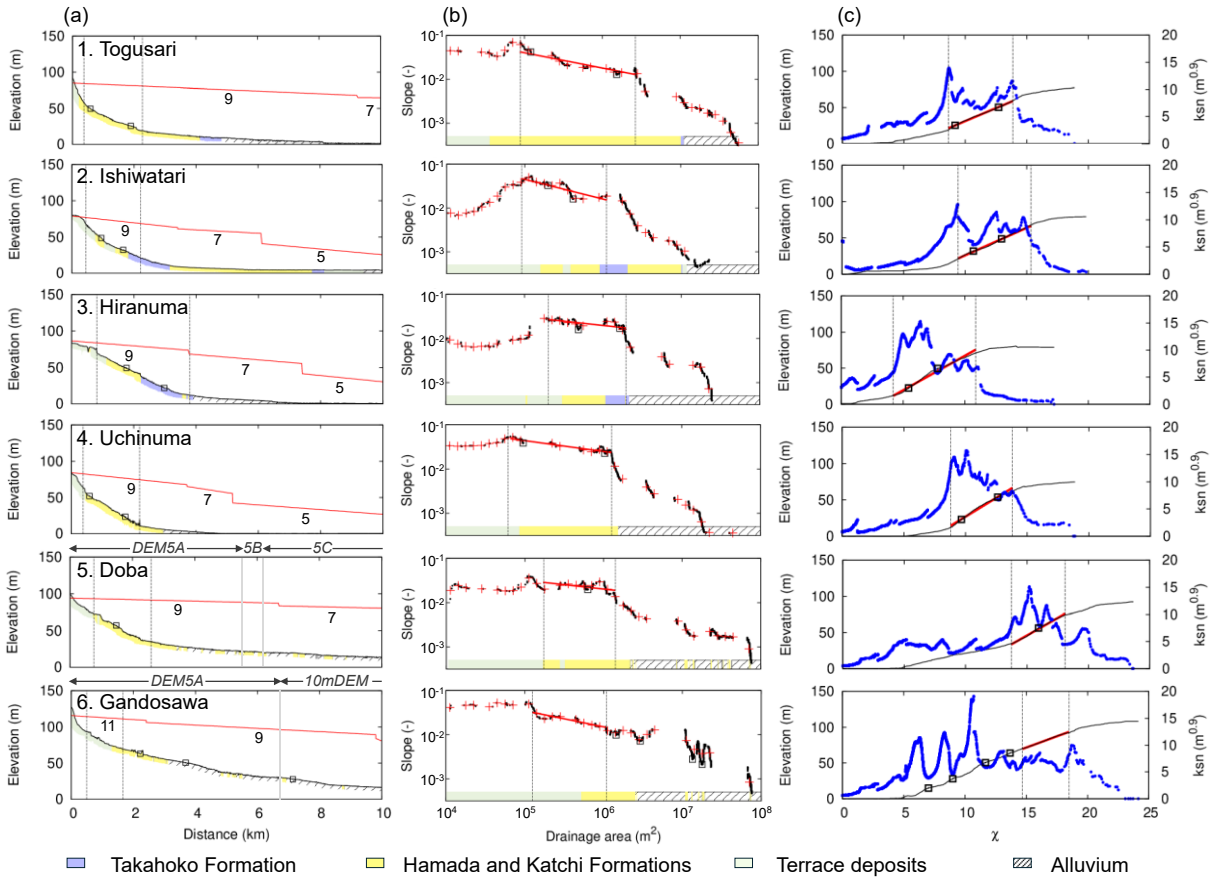

Figure 4: Stream profile analysis of the study area. (a) Longitudinal profile (black line) and the elevation of marine terraces (red line) with Marine Isotope Stages. Squares denote knickpoints. Gray lines for rivers No. 5 and 6 indicate the boundaries of DEMs other than DEM5A (LiDAR 5m DEM). (b) Slope-area plot. Average channel slopes are calculated on 5-m contours (black point) and by the log-bin averaging method (red mark). (c) χ plot (black line) based on the reference concavity ($\theta = 0.45$) with k_{sn} (blue point).In all graphs, dashed lines and red bold lines correspond to the bedrock section and its regression line.

[Revision]

Table 3: Formation ages and concavity indices (with standard deviation).

No.	1	2	3	4	5	6
Formation Age	MIS 9	MIS 9	MIS 9	MIS 9	MIS 9	MIS 11
θ	0.30 ± 0.06	0.18 ± 0.04	0.59 ± 0.04	0.29 ± 0.05	0.25 ± 0.15	0.56 ± 0.03

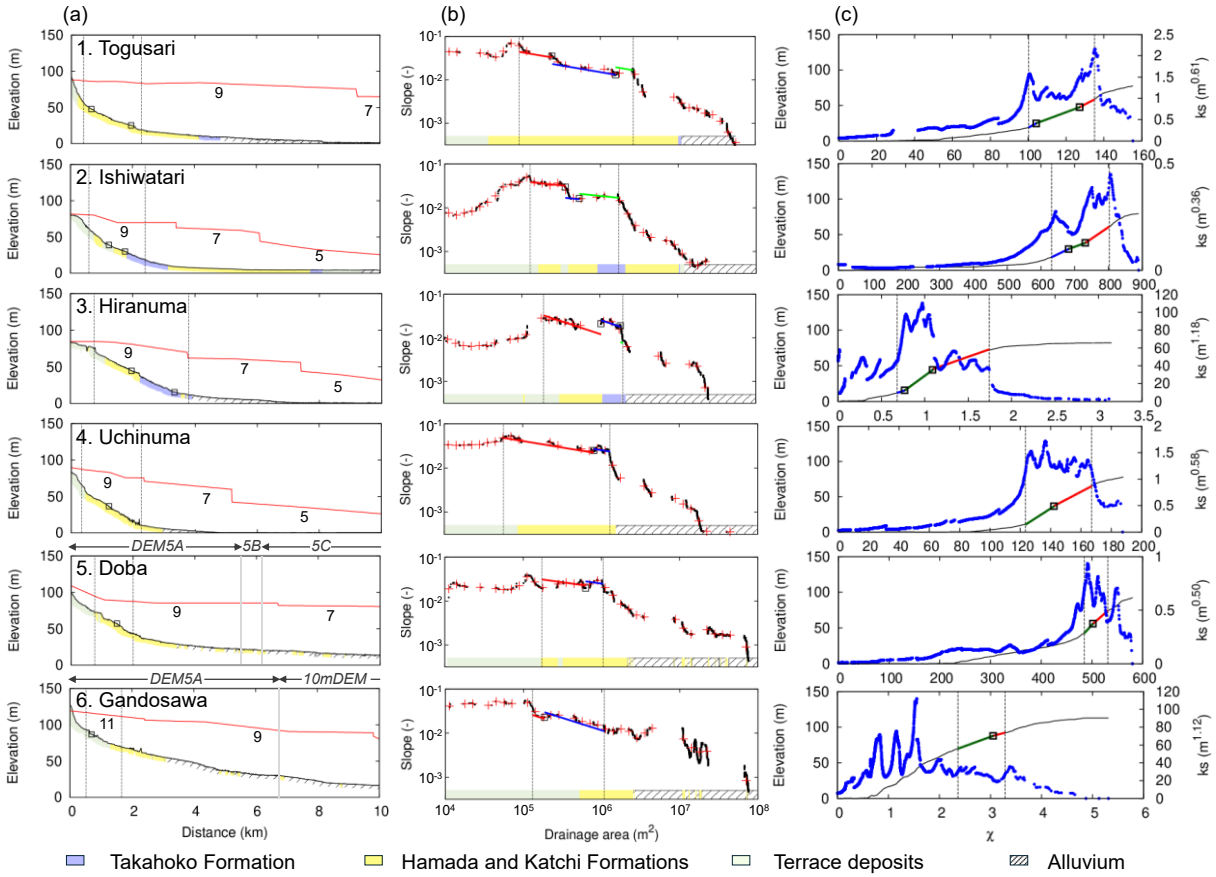

Figure 4: Stream profile analysis of the study area. (a) Longitudinal profile (black line) and the elevation of marine terraces (red line) with Marine Isotope Stages. Squares denote knickpoints. Gray lines for rivers No. 5 and 6 indicate the boundaries of DEMs other than DEM5A (LiDAR 5m DEM). (b) Slope-area plot. Average channel slopes are calculated on 5-m contours (black point) and by the log-bin averaging method (red mark). (c) χ plot (black line) with k_s (blue point) based on the concavity of each river. In all graphs, dashed lines and color bold lines (red, blue, and green) correspond to the bedrock section and its regression line.

In addition, we have added the figure of AICc for all rivers as Supplementary Material as follows.

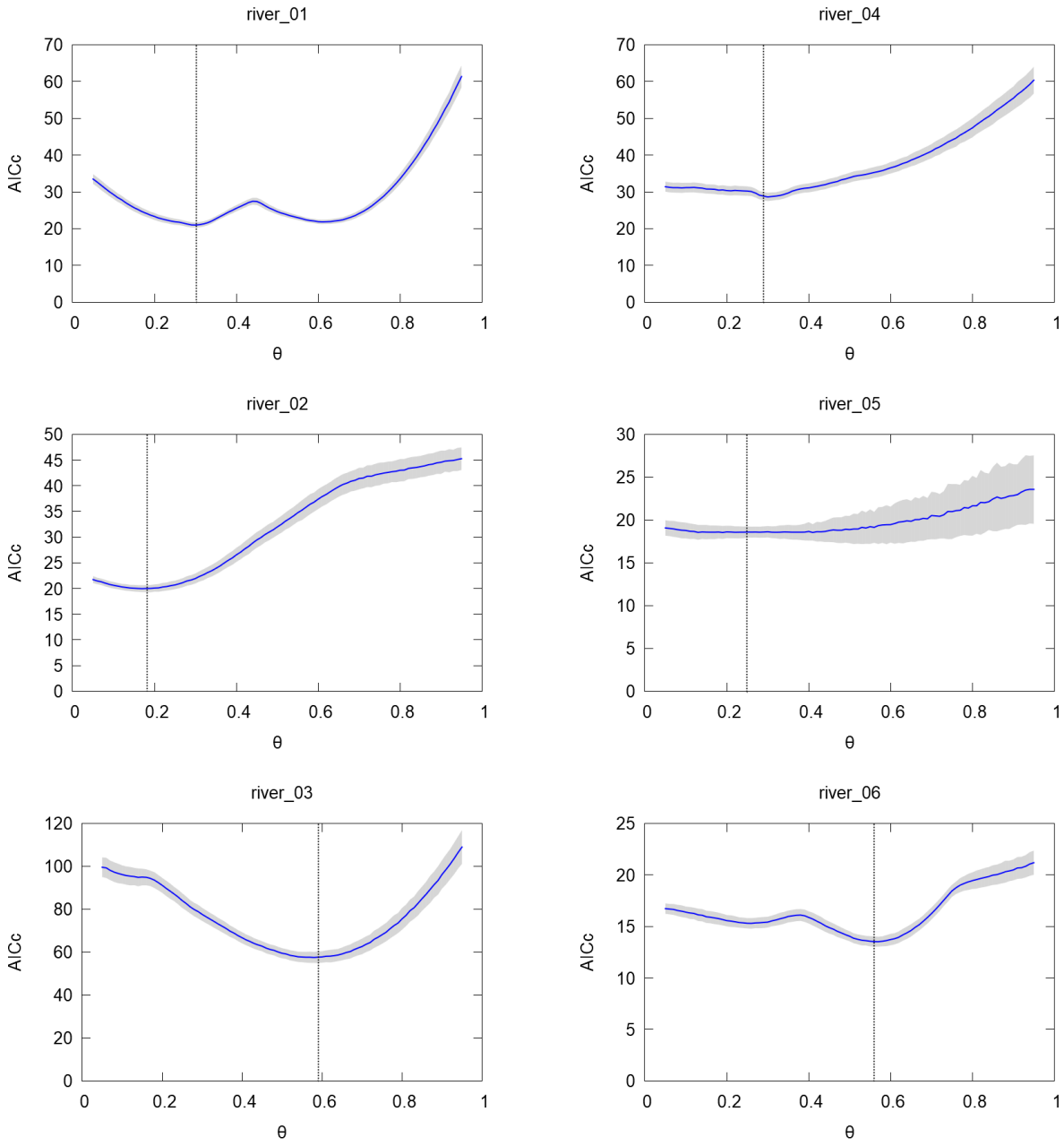

Figure S8: AICc values for each target river.

Knickpoints were extracted using the segment-fitting algorithm. The results confirm that the knickpoints do not coincide with lithological boundaries, with the exception of the second knickpoint of river No. 2. Instead, they are distributed at similar elevations (around 25 m and 50 m), which is consistent with the original manuscript. Based on these updated results, we have revised the Results section and added Table 4 (list of extracted knickpoints) as follows:

- Line 211-220 (new line 256–269)

[Original]

Figure 6 shows a map of the extracted knickpoints from the χ plots (Fig. 4c). The knickpoints are distributed at similar elevations (around E.L. 25 m and 50 m), which do not correspond to the lithology or the boundary of the different DEMs. This suggests that they can be base-level-fall related upstream-migrating knickpoints. In the Sanriku Coast, approximately 50 km south of the study area, Ogami (2015) indentified upstream-migrating knickpoints in multiple rivers which were formed during the sea-level highstands during MIS 5e, 7, 9, and 11. The knickpoints in the study area may have been formed for the same reason.

Note that lithological boundaries do not correspond to the knickpoints (Fig. 4). This is in agreement with the small difference in q_u of the bedrock, around several MPa, as discussed in Sect. 5.2. Another possible reason is sediment cover and tool effects (Yamanashi and Naruse, 2025). However, while the influence of the sediment requires further investigation, the cover and tool effects by riverbed gravel is considered to be insignificant for the target soft sedimentary rocks with q_u = 1–10 MPa.

[Revision]

Table 4 and Figure 6 show the extracted knickpoints and their locations on the map (Fig. 4c). All knickpoints are classified as slope-break knickpoints and do not correspond to the boundaries between different DEM datasets. Except for the second knickpoint of river No.2, the knickpoints are not located near lithological boundaries. Instead, they are distributed at similar elevations (around E.L. 25 m and 50 m). This suggests that they can be base-level-fall related upstream-migrating knickpoints. In the Sanriku Coast, approximately 50 km south of the study area, Ogami (2015) indentified upstream-migrating knickpoints in multiple rivers which were formed during the sea-level highstands during MIS 5e, 7, 9, and 11. The knickpoints in the study area may have been formed for the same reason. Note that in river No. 6, which formed earlier than the other rivers (MIS11), a knickpoint is observed at a higher elevation of 88 m. This knickpoint could have been formed during a preceding sea-level cycle.

The second knickpoint of river No.2 is located near the boundary between the Hamada and Katchi Formations and the Takahoko Formation (Fig. 4a). As discussed in Sect. 5.2, the Takahoko Formation exhibits higher *N*-values (80–137) compared with the Hamada and Katchi Formations (50–63). This contrast in rock hardness likely contributed to the formation of this lithological knickpoint. The same boundary is also located near the first knickpoint of river No.3; however, because its elevation is close to 50 m, this knickpoint might be affected by both the lithological difference and sea-level changes.

[Original] [Revision]

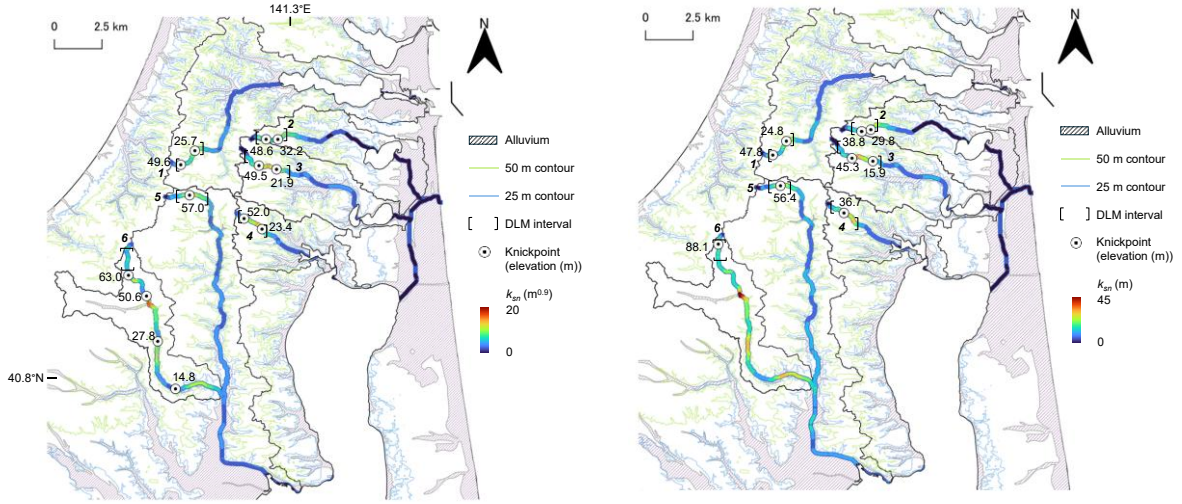

Figure 6: Knickpoints (points with elevation (m)) and 25 m and 50 m contours (blue and green lines) within the detachment-limited reaches. Color along the rivers demonstrates k_{sn} ($\theta_{ref} = 0.5$).

Table 4: Extracted knickpoints.

River No.	Knickpoint	Elevation (m)	Z_{jump} (m)	S_{ratio} (-)
1	Slope-break	47.8	-0.05	0.71
	Slope-break	24.8	0.05	1.49
2	Slope-break	38.8	-0.13	0.53
	Slope-break†	29.8	0.02	1.34
3	Slope-break	45.3	-0.71	2.10
	Slope-break	15.9	-0.04	0.44
4	Slope-break	36.7	-0.50	1.22
5	Slope-break	56.4	0.11	1.24
6	Slope-break	88.1	0.01	1.41

†This knickpoint is located approximately 50 m upstream from the lithological boundary (Hamada/Katchi and Takahoko Formations) along the river channel.

#2-4

I would like to see a comparison of ksn estimates between the values computed with the average theta and those computed with the individual theta values from each river.

Thank you for this constructive suggestion. We have addressed this by clarifying our use of individual versus reference theta values, depending on the specific objectives of each analysis:

1. Local analysis and knickpoint identification (Fig. 4c): Following Gailleton et al. (2019), we used the optimal θ for each river to identify knickpoint locations. This ensures that knickpoint extraction is not biased by a fixed θ_{ref}.

2. Spatial distribution map (Fig. 5): This map shows the spatial distribution of k_{sn} ($\theta_{ref} = 0.5$). This allows for a direct comparison of channel steepness across multiple rivers.

3. Estimation of parameters n and K (Fig. 7): As mentioned in our response to your earlier comment [#2-3], the estimated θ_{ref} for the study area is 0.44 ± 0.10. Since a consistent reference concavity is required to estimate n and K across different basins, we performed a sensitivity analysis using θ_{ref} = 0.4, 0.5, and 0.6 to ensure the robustness of our results.

As shown in Fig. 7, the choice of θ_{ref} did not fundamentally change our primary findings:

- Using the data points at 200 m intervals along the channels, we obtained $n > 1$.
- Using mean values averaged over detachment-limited reaches, we consistently obtained $n \sim 1$.

Minor comments:

#2-5 [Figure 3]

It is difficult to distinguish between vertical-step and slope-break knickpoints in Figure 3a.

Thank you for your comment. As detailed in our response to your earlier comment [#2-3], we have added a new table (Table 4) summarizing the extracted knickpoint types, alongside the elevation and slope change values for each knickpoint.

#2-6 [Figure 7]

Please explain what the dashed curve represents.

Thank you for pointing this out. We have updated the caption of Fig. 7 to the meaning as follows:

[Addition]

Figure 7: River incision rate versus channel steepness index k_{sn} within the detachment-limited reaches: (a-c) sampled at 200 m intervals and (d-f) averaged for each reach, both for θ_{ref} = 0.4, 0.5, and 0.6. Error bars denote ±1σ. The bold and dashed lines indicate the regression lines and their 90% confidence intervals.

Additional Amendments:

In addition to the above comments, the following amendments have been made.

[Abstract]

In response to the reviewers' comments, we have revised the abstract as follows within the 250-word limit:

[Revision]

Understanding river incision model is crucial for predicting long-term landscape evolution. For the bedrock channel incision model (detachment-limited (DL) model: erosion rate $E = KA^mS^n$ where A is drainage area, S is channel gradient), parameters (K, m, and n) can be estimated via slope-area analysis if E is known. Using ^{10}Be denudation rate, previous studies globally compiled the parameter values for variable lithology. However, limited data availability for soft sedimentary rock restricts the applicability of global compilation. In addition, measuring the ^{10}Be concentration in sedimentary rock is challenging in humid and tectonically active regions. To address this, slope-area analysis was conducted in the Kamikita Coastal Plain, Japan, where lithology (Miocene to Pleistocene sedimentary rocks) and uplift rate (~ 0.2 mm y^{-1} for the past 300 ka) are assumed to be uniform. River incision rates were derived approximately from widely distributed marine terraces (MIS 5e–11). For six target rivers, DL-like behaviour was confirmed in the limited areas located upstream of the alluvium distribution. The reference concavity m/n was 0.44 ± 0.10, typical for steady-state channels. Across the m/n range of 0.4–0.6, the exponent n consistently exhibited nonlinearity ranging between 1.14 to 1.34, which is consistent with the previous global compilations. This observed nonlinearity likely reflects transient landscape responses to past sea-level changes, which generated slope-break knickpoints at similar elevations. Finally, the estimated erosion coefficient K (10^{-5}–10^{-6}) agreed with the global relationship with unconfined compressive strength q_u ($K \propto 1/q_u^2$), supporting the significant influences of bedrock lithology on K.

[Line 84–89 (new line 91-96)]

We have added detailed lithological descriptions for each unit as follows:

[Revision]

Bedrock was formed in the early to middle Miocene: the Takahoko Formation, sedimentary rock (16.6–13.1 Ma), which is mainly composed of pumice tuff, sandstone, and mudstone (Inohara et al., 2008), and the Tomari Formation, volcanic rock (16.6–15 Ma), characterized by basaltic to andesitic lavas and pyroclastic rocks (Kudo et al., 2020). Sedimentary rock units of late Pliocene to early Pleistocene, the Hamada Formation and the Katchi Formation, which primarily consist of sandstone and siltstone (Nemoto and Ujiie, 2009), overlay the bedrock.

We have also added the following references:

Inohara, Y., Oyama, T., and Torigoe, Y.: Magnetic Susceptibility Analysis of Takahoko Formation at Simokita Peninsula, Northeast Japan, J. Jpn. Soc. Eng. Geol., 49, 3, 139–149, https://doi.org/10.5110/jjseg.49.139, 2008 (in Japanese with English summary).

Nemoto, N. and Ujiie, Y.: Geology of Aomori prefecture, in: Daichi, Tohoku Geotechnical Consultants Association, Miyagi, Japan, 52–68, https://tohoku-geo.ne.jp/information/daichi/img/50a/52.pdf (last access: 17 April 2026), 2009 (in Japanese).

[Line 104 (new line 111)]

We have added the size of drainage area of Takase River as follows:

[Addition]

Note that the rivers No. 2–6 are tributaries of the Takase River, which has a drainage area of 867 km^2 (MLIT, 2006) and flows from…

We have also added the following reference:

MLIT (Ministry of Land, Infrastructure, Transport and Tourism of Japan): River improvement plan of Takase River, https://www.thr.mlit.go.jp/takase/committe/keikaku/pdf/keikaku.pdf (last access: 13 April 2026), 2006 (in Japanese).

[New line 163]

We have added the range of concavity estimation as follows:

[Addition]

In the second step, we calculated the channel concavity index from the integral approach within the detachment-limited reaches (Perron and Royden, 2013):

[New line 211]

We have added the locations of outcrop observations for tephra thickness in the Supplement Material (Fig. S7) as follows:

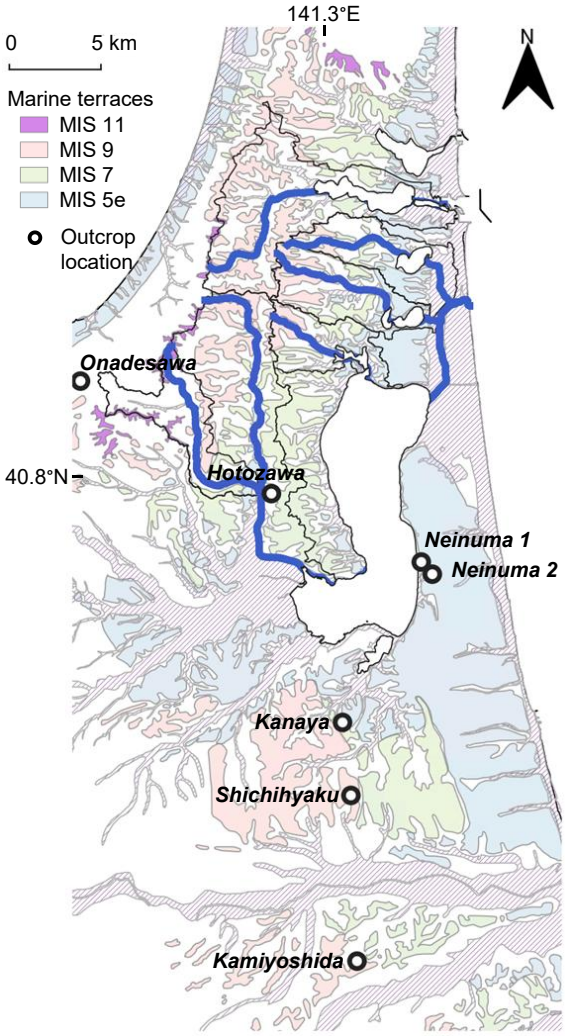

Figure S7: Outcrop locations investigated by AIST (2015, 2016).

[Line 274–281 (new line 348–360)]

We have revised the discussion regarding the underestimation of K. A third reason related to cohesion has been added based on the lithological features of the main riverbed lithologies, as follows:

[Original]

However, the results of this study underestimate K (the regression line) in the work of Haag and Schoenbohm (2025). One possible reason for this discrepancy is the effect of sea-level change, which is discussed in Sect. 5.1. When comparing the average k_{sn} and E in the river section, a larger K of 8.9×10^{-6} [4.7×10^{-7}, 1.7×10^{-4}] $m^{0.1}\ y^{-1}$ was obtained (Fig. 8). Although the estimation uncertainty is large, the estimated K value is consistent with the relationship described by Haag and Schoenbohm (2025). Another possible reason for the discrepancy is that we compared the present values of k_{sn} with long-term average erosion rates. Since the target rivers have been formed gradually by incising the flat marine terraces, long-term average k_{sn} should be less than the present value. If the long-term average k_{sn} is half of present k_{sn}, the estimated K doubles without changing the n value.

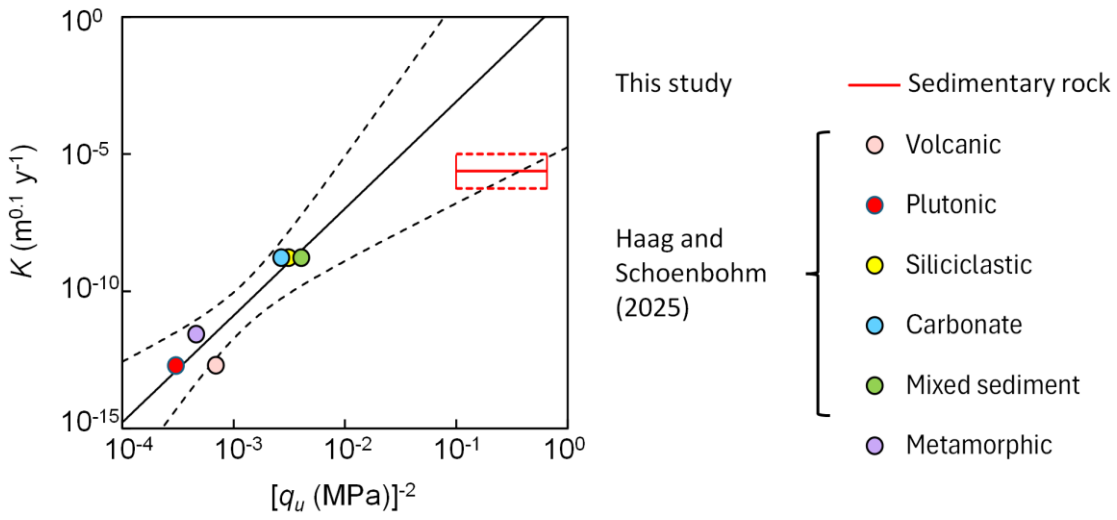

Figure 9: Comparison between the results of this study and data of Haag and Schoenbohm (2025) (color points) for unconfined compressive strength q_u and erosional coefficient K. The box plot shows the best estimate and 90% confidence interval of our results based on the log-bin averaged data for all the rivers. The black line and dashed lines are the best estimate and 90% confidence interval shown in Haag and Schoenbohm (2025).

[Revision]

However, the results of this study underestimate K (the regression line) in the work of Haag and Schoenbohm (2025). This discrepancy is likely caused by three potential reasons. First, as discussed in Sect. 5.1, the influence of sea-level changes may lead to an underestimation of K. When comparing the average k_{sn} and E in the river section, which effectively smooths the transient knickpoint migration due to sea-level changes, the estimated K value increased to 6.2×10^{-6} [7.7×10^{-8}, 5.1×10^{-4}], approaching the relationship described by Haag and Schoenbohm (2025) (Fig. 9).

Second, the discrepancy may arise from the use of present values of k_{sn} to compare with long-term average erosion rates. Since the target rivers have been formed gradually by incising the flat marine terraces, long-term average k_{sn} should be less than the present value. If the long-term average k_{sn} is half of present k_{sn}, the estimated K doubles without changing the n value.

Third, the cohesion of the main riverbed lithologies (the Hamada and Katchi Formations), which are semi-consolidated sedimentary rocks with q_u =1.2–3.1 MPa that primarily consist of sandstone and siltstone (see Sect. 2), may function as a resistive factor. This cohesion increases the shear stress threshold and leads to the dissipation of stream power. Since standard mechanical indicators such as N-values often fail to fully capture the cohesive resistance inherent in these semi-consolidated units, the resulting K values may fall near the lower bound of the global relationship.

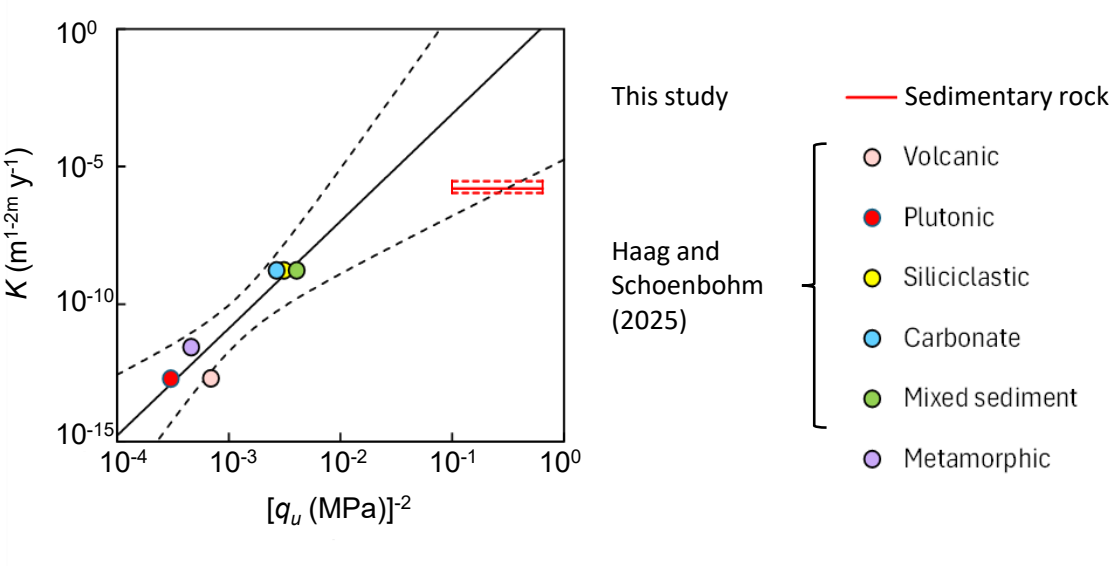

[Line 294–298 (new line 373–378)]

In response to the reviewers' comments, we have revised the Conclusion section as follows:

[Original]

(1) DL-like behaviour was confirmed in the limited upstream and midstream area ($A \geq 10^{-5}$ km^2) located upstream of the alluvium distribution for all rivers. Except for small rivers of $A < 25$ km^2, the concavity index m/n was between 0.35 and 0.6, which is the typical range for steady-state channels.

(2) Exponent n was nonlinear, ranging between 1 and 2, which is consistent with the previously global compilation. This nonlinearity can be due to past sea-level changes, causing knickpoints at similar elevations.

[Revision]

(1) DL-like behaviour was confirmed in the limited upstream and midstream area ($A \geq 10^{5}$ m^2) located upstream of the alluvium distribution for all rivers. Although the optimal θ value varied from 0.18 to 0.59 for each river, θ_{ref} was estimated to be 0.44 ± 0.10, which falls within the typical range for steady-state channels (0.35–0.6).

(2) Across the θ_{ref} range of 0.4 to 0.6, exponent n consistently exhibited a nonlinear relationship, ranging between 1.14 and 1.34, which aligns with the previous global compilation of 1 to 2. This nonlinearity can be due to past sea-level changes, causing slope-break knickpoints at similar elevations.

[Throughout the manuscript]

- The subscript "ref" in θ_{ref} has been consistently italicized throughout the manuscript.
- The unit of K has been changed from m$^{0.1}$ y^{-1} to m^{1-2m} y^{-1}.